Tunneling through equivalent multihumped fission barriers: Some implications for the actinide nuclei

B. S. Bhandari and A. S. Al-Kharam
Department of Physics and Astronomy, Faculty of Science, University of Garyounis, Benghazi, Libya
(Received 17 March 1988)

A comparison of the penetrabilities calculated in the Wentzel-Kramers-Brillouin approximation through equivalent multihumped fission barriers shows that the penetrability saturates to its maximum value much more slowly for a three-humped potential than that for comparable two-humped and single-humped potentials. An analysis of the slopes of the near-barrier photofission cross sections of actinides yields results that can be understood in terms of the predicted potential barrier shapes for these nuclei, and thus provides evidence in support of resolving the "thorium anomaly" along the lines suggested by Möller and Nix. Our results further indicate that the uranium nuclei, and in particular ^{236}U, may more likely exhibit three-humped potential shapes in which the apparent consequences of both the second and third minima may be observable.

I. INTRODUCTION

The studies of the detailed shapes of the potential barriers against fission of heavy nuclei have been of considerable interest over the past two decades.[1-7] While most of the medium heavy fissioning nuclei exhibit a single-humped potential barrier against fission as predicted by the liquid drop model,[8] those in the actinide region have been found to exhibit a double-humped potential barrier. Such barriers have been shown[1] to occur mainly as a result of the superimposition of the oscillatory "shell corrections" or the so-called single-particle effects on the relatively flat potential energy surfaces predicted by the liquid drop model in the corresponding deformation regions for the actinide nuclei. For the lighter actinides, such as those in the thorium region, the inclusion of the mass-asymmetric deformations in the fission barrier calculations led[4] to a further splitting of the outer or the second barrier in two, thereby indicating a triple- or a three-humped potential barrier against fission. A close examination of the potential energy surfaces in these cases reveals that there are, in fact, two third wells, in which the fissioning compound nucleus has equal quadrupole deformations, but opposite "pear-shaped" octupole deformations. These two wells are separated by a low barrier of about 1 MeV along the mass-asymmetry degree of freedom. Such potentials with rather shallow third minima have been suggested[4] as a possible explanation of the so-called "thorium anomaly" in fission literature. This anomaly consists of a systematic discrepancy in the theoretically calculated heights of the inner (or the first) barriers and of the second minima with their values obtained experimentally for most of the actinides[5] with neutron numbers $N \lesssim 140$. On the other hand, for the very heavy actinides with $N > 154$, some evidence has been reported[9] suggesting even a fragmentation of the inner or the first peak of the fission barrier.

Extensive experimental evidences have been reported in fission literature over the past two decades in favor of such complex potential barrier shapes for the actinide nuclei. While a host of experimentally observed phenomena such as narrow and broad resonance structures in subbarrier fission cross sections, fission isomers, and the so-called "isomeric shelf," observed in the deep subbarrier photofission cross sections of the actinide nuclei, provide ample evidence in favor of two- and three-humped potential barriers as against a single-humped potential barrier, it has not yet been possible to conclusively differentiate between a two-humped and a three-humped potential barrier for the actinide nuclei based exclusively on the observed experimental data. The observation of rather narrow resonances in the neutron-induced fission cross sections of ^{230}Th and ^{232}Th by the Saclay group[10-12] provide so far the most direct evidence in favor of a three-humped potential barrier. Fine structures observed within these resonances in high-resolution measurements have been interpreted as corresponding to rotational band structures of opposite parity built on the relatively undamped vibrational states in the dual third minima. The band head separation of these opposite parity structures is determined by the penetrability of the low barrier separating the two third minima. However, Lynn[13] has shown that the observed structure could also result from the coupling of single-particle and vibrational motion in these nuclei and has further considered the effects of the coriolis interaction on such structures more recently.

Central to the description of subbarrier fission process in terms of such multihumped fission barriers is the quantitative calculation of the probability that a fissioning nucleus shall tunnel through such complicated potential barriers. Penetrability calculations through such potential shapes have been reported by several authors and have been used extensively in the analysis of the observed subbarrier fission phenomena at various laboratories. The purpose of the present manuscript is to critically compare the results of such penetrability calculations through a few equivalent sets of a single-, a double-, and a triple-humped potential barriers in order to investigate the resulting differences expected in the correspondingly calculated subbarrier fission cross sections. It is hoped that such a study may suggest some clues which, when compared with the observed subbarrier fission cross sec-

tions of suitable nuclei, might help in differentiating between a two-humped and a three-humped potential barrier in the lighter actinides.

II. FISSION PENETRABILITY CALCULATION

Penetrability calculations through multihumped potential barriers have acquired special significance in recent years because of the fact that most of the fissionable actinide nuclei are now known to exhibit two- or three-humped fission barriers. As most of the interesting physics of low energy (subbarrier) fission is determined by the probability that the fissioning compound nucleus shall tunnel through its corresponding fission barrier, it is important to calculate the tunneling probability through such potential shapes. These penetrability calculations can be carried out in Wentzel-Kramers-Brillouin (WKB) or quasiclassical approximation,[14–21] numerically,[22] and also exactly[23–29] if the potential shapes in the individual regions are approximated by parabolas or some other suitable shapes for which the corresponding Schrödinger equation can be solved exactly. The analytical expressions for the penetrability through such potential barriers derived in the WKB approximation, however, provide interesting physical insight into the problem and can be used more effectively for the analyses of the measured data on the intermediate structure in the second well as emphasized recently in a photofission investigation.[30] Also, as the method is applicable for a wide variety of suitably parametrized arbitrary potential shapes and also for a reasonably wide range of incident energies, we have resorted to this approximation in the present work. The detailed calculations of the penetrability through such potential shapes in WKB approximation have already been reported [except the Eq. (12)] by us[17–20] as well as by other authors[14–16,21] in the past, and, therefore, we only quote here the analytical expressions for the penetrability and compare the results obtained using these expressions for the equivalent set(s) of such multihumped potential barriers.

A. Analytical expressions for the penetrability

1. Single-humped barrier

For an arbitrary-shaped potential barrier [Fig. 1(a)] of height E_0 and curvature energy $\hbar\omega_0$, the penetrability calculated in the JWKB approximation by Fröman and Fröman[15] is given as

$$P=[1+\exp(2\nu)]^{-1} \tag{1}$$

for energies below the top of the barrier, and

$$P=[1+\exp(-2|\nu|)]^{-1} \tag{2}$$

for energies above the top of the barrier. The energy-dependent phase ν is given as

$$\nu=\int_a^b\{2\mu[V(\epsilon)-E]/\hbar^2\}^{1/2}d\epsilon\ , \tag{3}$$

where μ is the effective mass of the tunneling system along the ϵ direction, $V(\epsilon)$ is the potential as a function

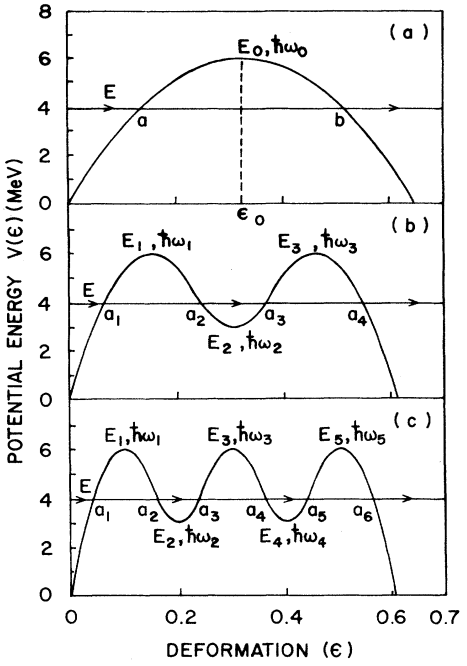

FIG. 1. An equivalent set of single-, double-, and triple-humped symmetric potential barriers. The barrier parameters are given in the following. Other symbols are described in the text. Single-humped: $E_0=6$ MeV, $\hbar\omega_0=0.485$ MeV. Double-humped: $E_1=E_3=6$ MeV, $E_2=3$ MeV, $\hbar\omega_1=\hbar\omega_2=\hbar\omega_3=1.018$ MeV. Triple-humped: $E_1=E_3=E_5=6$ MeV, $E_2=E_4=3$ MeV, $\hbar\omega_1=\hbar\omega_2=\hbar\omega_3=\hbar\omega_4=\hbar\omega_5=1.55$ MeV.

of the dimensionless deformation parameter ϵ, and E is the total energy of the system. a and b are the two classical turning points where $E=V(\epsilon)$. Since ϵ is dimensionless, μ has the dimensions of the moment of inertia. The value of μ used in the present work has been taken to be constant for all values of ϵ, and is taken to be equal to[23]

$$\mu=0.054A^{5/3}\hbar^2\ \text{MeV}^{-1}\ , \tag{4}$$

where $\hbar$ is to be expressed in MeV sec and A is the nuclear mass number. E_0 is the maximum value of the potential, $V(\epsilon)$, at the deformation ϵ_0.

For a parabolic single-humped potential barrier, Hill and Wheeler[29] have derived an exact expression for the penetrability as

$$P=\{1+\exp[2\pi(E_0-E)/\hbar\omega_0]\}^{-1}\ . \tag{5}$$

This formula gives results exactly identical to those given by Eq. (1) for a parabolic potential barrier.

2. Double-humped barrier

Defining P_A, P_B, and P as the respective penetrabilities for the first barrier alone, second barrier alone, and the entire double-humped barrier, it has been shown[17–20] that

$$P=P_AP_B/(\{1+[(1-P_A)(1-P_B)]^{1/2}\}^2\cos^2\nu_2 + \{1-[(1-P_A)(1-P_B)]^{1/2}\}^2\sin^2\nu_2)\ , \tag{6}$$

where the individual penetrabilities (P_A and P_B) in the WKB approximation are given[15] as

$$P_A=[1+\exp(2\nu_1)]^{-1}\ ,\qquad P_B=[1+\exp(2\nu_3)]^{-1}\ , \tag{7}$$

for energies below the top of the barriers, and

$$P_A=[1+\exp(-2|\nu_1|)]^{-1}\ ,\qquad P_B=[1+\exp(-2|\nu_3|)]^{-1}\ , \tag{8}$$

for energies above the top of the barriers. The quantities ν_i are the integrals in respective regions, as shown in Fig. 1(b), of the wave numbers or the momentum functions

$$K_1(\epsilon)=\{2\mu[E-V(\epsilon)]/\hbar^2\}^{1/2}=iK_2(\epsilon)\ , \tag{9}$$

for example,

$$\nu_1=\int_{a_1}^{a_2}K_2(\epsilon)d\epsilon\ ,\quad \nu_2=\int_{a_2}^{a_3}K_1(\epsilon)d\epsilon\ ,\quad \nu_3=\int_{a_3}^{a_4}K_2(\epsilon)d\epsilon\ . \tag{10}$$

The classical turning points a_1, a_2, a_3, and a_4 are as shown in Fig. 1(b) for an incident energy E. For the actual computation of the penetrability, the double-humped potential barrier has been parametrized by smoothly joining three parabolas and is given by

$$V(\epsilon)=E_j\pm\tfrac{1}{2}\mu\omega_j^2(\epsilon-\epsilon_j)^2\ , \tag{11}$$

where the plus sign applies for $j=2$ and the minus sign for $j=1$ and $j=3$. E_j represent the maxima and minima of the potential, $\hbar\omega_j$ their respective curvature energies, and ϵ_j the locations of the extrema on the deformation axis. $V(\epsilon)$ is taken to be zero at $\epsilon=0$. The value of μ used in the calculation is as given in Eq. (4).

3. *Triple-humped barrier*

Defining P_A, P_B, P_C, and P as the respective penetrabilities for the first barrier alone, the second barrier alone, the third barrier alone, and the entire three-humped potential barrier, it has been shown[20] through a straightforward, though rather tedious, analytical formalism that

$$\begin{aligned}P=P_AP_BP_C/([1+(1-P_A)(1-P_B)+(1-P_A)(1-P_C)+(1-P_B)(1-P_C)]\\ +\{2(2-P_C)[(1-P_A)(1-P_B)]^{1/2}\}\cos(2\nu_2)+\{2(2-P_A)[(1-P_B)(1-P_C)]^{1/2}\}\cos(2\nu_4)\\ +\{2(1-P_B)[(1-P_A)(1-P_C)]^{1/2}\}\cos[2(\nu_2-\nu_4)]+\{2[(1-P_A)(1-P_C)]^{1/2}\}\cos[2(\nu_2+\nu_4])\ ,\end{aligned} \tag{12}$$

where the individual penetrabilities (P_A, P_B, and P_C) are given in the WKB approximation by expressions similar to those given earlier. For example, P_A and P_B are exactly as defined in Eqs. (7) and (8), respectively, while P_C is given as

$$P_C=[1+\exp(2\nu_5)]^{-1} \tag{13}$$

for energies below the top of the barrier, and

$$P_C=[1+\exp(-2|\nu_5|)]^{-1} \tag{14}$$

for energies above the top of the barrier. The quantities ν_i are the integrals in the respective regions, as shown in Fig. 1(c), of the wave numbers or the momentum functions defined in Eq. (9). For example, in addition to the ν_1, ν_2, and ν_3 as defined in Eq. (10), we also have

$$\nu_4=\int_{a_4}^{a_5}K_1(\epsilon)d\epsilon,\quad \nu_5=\int_{a_5}^{a_6}K_2(\epsilon)d\epsilon\ . \tag{15}$$

The classical turning points a_1, a_2, a_3, a_4, a_5, and a_6 are as shown in Fig. 1(c) for an incident energy E. For the actual computation of the penetrability, the triple-humped potential barrier has been parametrized by smoothly joining five parabolas and is given by Eq. (11) where the plus sign now applies for $j=2$ and 4, and the minus sign for $j=1$, 3, and 5.

In the generalized JWKB approximation developed by Fröman and Fröman,[15] expressions for the penetrability have been obtained both at excitations below and above the top of the barriers as given earlier. This involves considering both the real as well as complex turning points. For the special case of a potential barrier parametrized by an inverted parabola of height E_0 and curvature energy $\hbar\omega_0$, i.e.,

$$V(\epsilon)=E_0-\tfrac{1}{2}\mu\omega_0^2(\epsilon-\epsilon_0)^2\ ; \tag{16}$$

the energy dependent phase ν can be obtained by a straightforward integration in Eq. (3) as

$$\nu=[\pi(E_0-E)/\hbar\omega_0]\ . \tag{17}$$

Similarly, for two- and three-humped barriers, the phases ν_j at energies above the top of the individual parabolic barriers are given as

$$|\nu_j|=|[\pi(E_j-E)/\hbar\omega_j]|\ , \tag{18}$$

where $j=1,3$, and 5.

These expressions have been used in calculating the penetrabilities at excitations above the top of the indivi-

dual parabolic barriers using the Eqs. (2), (8), and (14), respectively.

B. Results: Comparison of penetrabilities

For the equivalent one-, two-, and three-humped fission barriers shown in Figs. 1 and 2, we have calculated the penetrability using the above formulas and the results are shown in Figs. 3–5. By the term "equivalent" we mean that the three barriers (one-, two-, and three-humped) chosen for a given set give approximately the same penetrability at excitations close to the bottom of the potential and thus predict approximately similar spontaneous fission half-lives. A sample comparison of the calculated penetrabilities in the entire energy range (subbarrier) is shown in Fig. 3 for the set of three equivalent fission barriers of Fig. 1. The single-humped barrier penetrability increases monotonically with energy. On the other hand, the two-humped and the three-humped barrier penetrabilities exhibit narrow resonances. As the barriers chosen for this set are symmetric, the penetrability resonances rise to a maximum value of unity. Also seen in this figure are the so-called "doublets," expected in a symmetric triple-humped barrier as it is exactly similar to the problem of a symmetric double-well potential where such opposite parity states arise as a result of the removal of the otherwise two-fold degeneracy due to the tunneling through the finite intermediate barrier separating the two wells. While this splitting is too small to be seen for the lower resonance, it is clearly visible for the higher resonance in the three-humped barrier penetrability curve of Fig. 3.

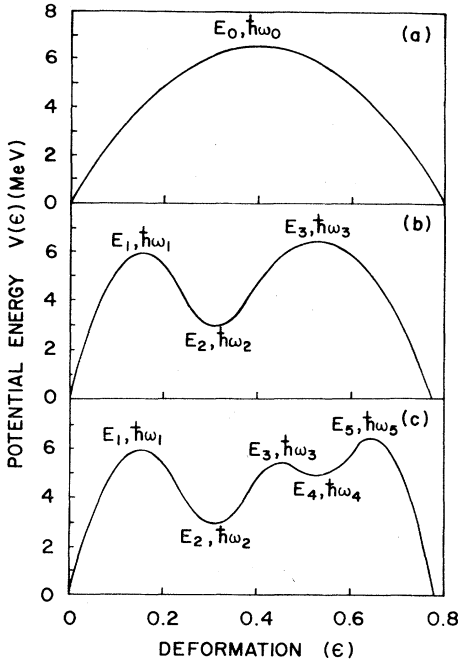

FIG. 2. An equivalent set of single-, double-, and triple-humped asymmetric potential barriers. The barrier parameters are given in the following. Single-humped: $E_0=6.5$ MeV, $\hbar\omega_0=0.406$ MeV. Double-humped: $E_1=6$ MeV, $E_2=3$ MeV, $E_3=6.5$ MeV, $\hbar\omega_1=1$ MeV, $\hbar\omega_2=1$ MeV, $\hbar\omega_3=0.66$ MeV. Triple-humped: $E_1=6$ MeV, $E_2=3$ MeV, $E_3=5.5$ MeV, $E_4=5$ MeV, $E_5=6.5$ MeV, $\hbar\omega_1=1$ MeV, $\hbar\omega_2=1$ MeV, $\hbar\omega_3=1$ MeV, $\hbar\omega_4=0.8$ MeV, $\hbar\omega_5=1.2$ MeV.

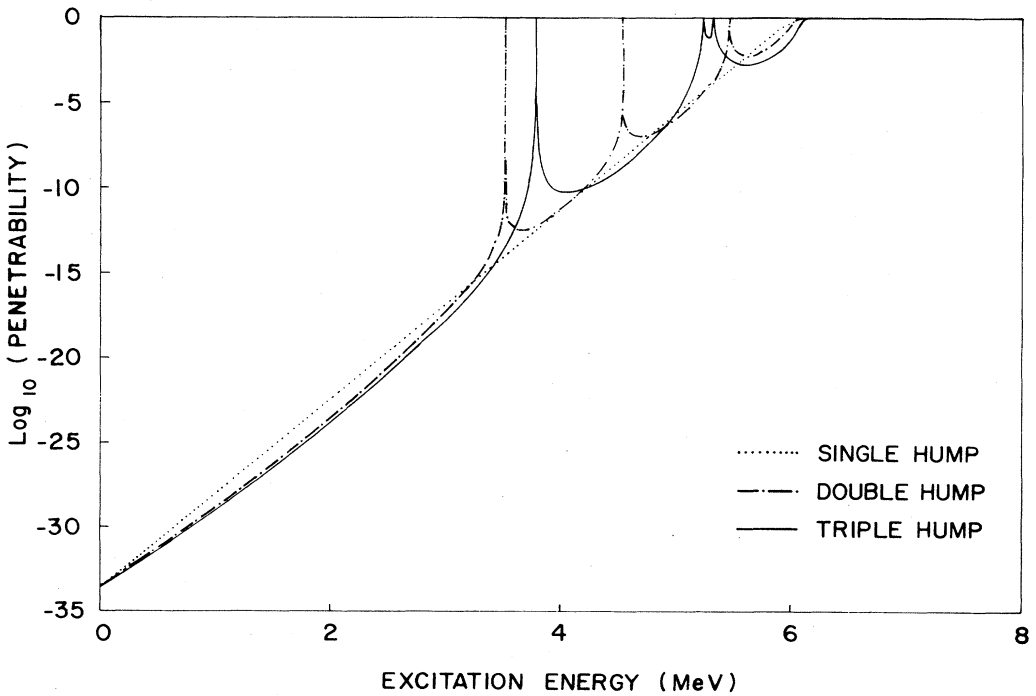

FIG. 3. A logarithmic plot of the penetrabilities through the equivalent set of single-, double-, and triple-humped potential barriers of Fig. 1 in the entire subbarrier energy region.

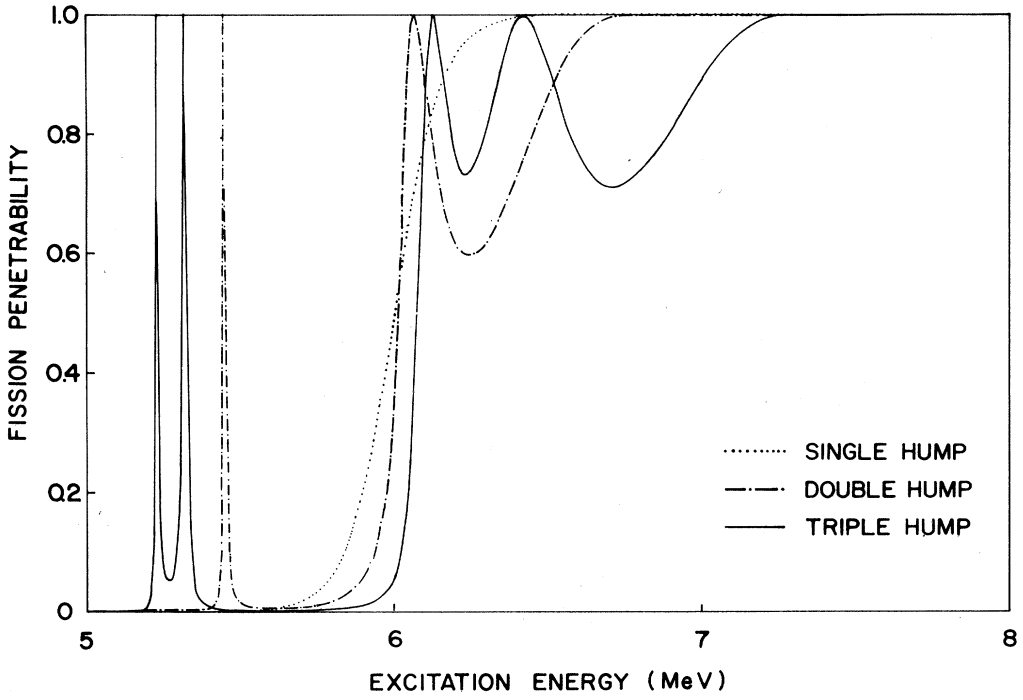

FIG. 4. A linear plot of the penetrabilities through the equivalent set of single-, double-, and triple-humped potential barriers of Fig. 1 in the energy region close to the top of the barriers.

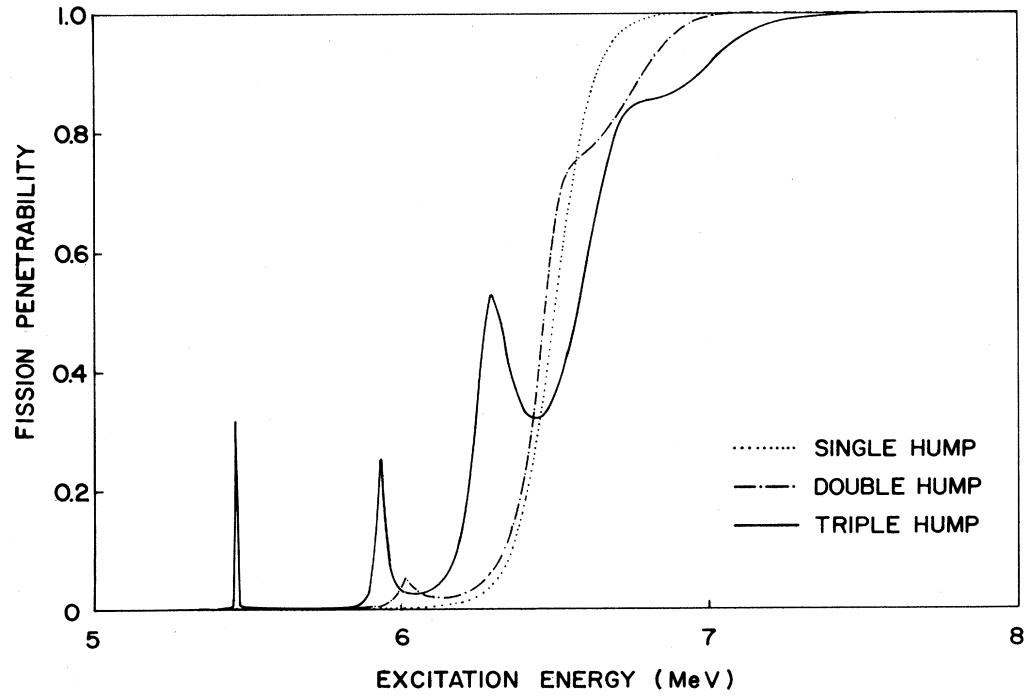

FIG. 5. A linear plot of the penetrabilities through the equivalent set of single-, double-, and triple-humped potential barriers of Fig. 2 in the energy region close to the top of the barriers.

In addition to the above expected features, and leaving aside the effects of the various resonances, we also observe that the single-humped barrier penetrability rises much more rapidly than that for a double-humped barrier and even more than that for a triple-humped barrier. This behavior is seen more clearly at excitations close to the top of the barriers and is shown in the linear plots of the penetrabilities in Figs. 4 and 5. In Fig. 4 the rapid rise of the penetrabilities corresponding to the double- and triple-humped barriers just below 6 MeV is caused by the presence of the transmission resonances in these potentials. This is not to be confused with the general behavior of the slopes of the corresponding penetrabilities. Above these resonance energies, it can be seen clearly in Fig. 4 that the three-humped barrier penetrability saturates to its maximum value much more slowly than that for the equivalent two-humped barrier, and even more slowly than that for the corresponding single-humped barrier. A similar feature is also observed in Fig. 5. This means that a triple-humped barrier will allow a much slower opening of the fission channels or transition states than would be the case for the equivalent double-humped and single-humped barriers. Such a feature was reported earlier by Cramer and Nix[23] while comparing the penetrabilities through the equivalent single- and double-humped fission barriers. As the same feature is now found between a double- and a triple-humped barrier, we shall attempt to exploit it to distinguish between the corresponding fission barriers in the actinide nuclei. The main influence of such a feature would be expected in the measured fission probabilities at excitations close to the top of the barriers. The slopes of the fission cross sections at such excitations would then be expected to be considerably smaller for a triple-humped fission barrier than those for an equivalent double-humped barrier. A systematic analysis of the slopes of the fission cross sections at energies close to the top of the fission barriers can then be expected to lead to some useful information that can help distinguish between a triple- and a double-humped fission barrier for a given actinide. Such an analysis of the photofission cross sections of the various actinide nuclei is discussed in Sec. III.

III. SLOPES OF THE NEAR-BARRIER PHOTOFISSION CROSS SECTIONS OF ACTINIDES

For a systematic analysis of the slopes of the fission cross sections at excitations in the vicinity of the top of the fission barrier, one can use the experimental data from the low energy neutron-induced fission, charged-particle- or direct-reaction-induced fission, and the photofission or the electron-induced fission. However, for the actinide nuclei, as the neutron binding energies are approximately equal to or even greater than the fission barrier heights, the neutron-induced fission data are only of limited use for such an analysis. The direct-reaction-induced fission data can be useful provided proper account is taken of the complexities due to a large variety of spin and angular momenta introduced by the exciting particle. In addition the effects of the Coulomb barriers on the slopes have to be taken into account for the charged-particle-induced fission data. Of course, the main advantages of these particle-induced fission data are the relatively large cross sections and thus more accurate measurements with very high energy resolutions of the order of a few keV.[12]

The photofission and electrofission processes are quite useful[31–33] especially because of the restricted angular momenta in the entrance channel corresponding mainly to the dipole and the quadrupole photoabsorption. This particular feature of the limited angular momenta in photofission processes was pointed out by Bohr[32] long before the realization of two- and three-humped fission barriers in actinide nuclei. Unfortunately the relative weakness of the electromagnetic interaction results in very low cross sections in photofission and electrofission processes, thus rendering such measurements extremely difficult. While some investigations have been reported using the neutron- and proton-capture gamma rays, bulk of the photofission studies have been made using the intense gamma flux in the electron bremsstrahlung beams from the low energy, high-current microtrons or the electron linear accelerators. The use of bremsstrahlung beams in such investigations introduces the usual problems associated with the unfolding of the measured yield curves obtained with a continuous gamma-ray spectrum and results in a relatively poor energy resolution. The use of the Chalk-River bremsstrahlung monochromator in a recent high-resolution photofission measurement[34] appears rather promising in this connection. The absolute photofission data obtained at different laboratories also differ—sometimes rather significantly, and thus call for caution in using such data.

A systematic compilation of the data on photofission cross sections of the actinide nuclei reported over the past 30 years has become available recently[35] and it was this ready availability of the data and the relative advantages of the restricted angular momenta in photofission processes that led us to choose the photofission cross sections for the present analysis. As far as possible, we have tried to use the data on various actinides obtained at the same laboratory so as to minimize the uncertainties associated with different experimental conditions and other systematic errors. The main competition to the fission process in the excitation region close to the fission barrier heights in the actinide nuclei comes from the neutron emission and as we are interested in the slopes of the fission probability alone, the data used for the present analysis has in most cases been restricted to energies below the neutron binding energies. Of course, at excitations well below the top of the fission barriers the cross sections will exhibit an exponential increase with energy and thus only a small energy region typically of the order of an MeV below the neutron binding energies and in the close vicinity of the fission barriers is really suitable for a linear "fit" of the photofission cross sections in order to extract their slopes. Our procedure for a typical nucleus consisted of beginning initially with the entire set of available data up to an energy just below the neutron binding energy in the nucleus and then progressively reducing the total number of data points one by one at the

TABLE I. Relevant details of the near-barrier photofission cross-section data used in a linear least-squares analysis to extract their slopes. All of the above data has been taken from the recent numerical compilation in Ref. 35. The original references are listed in the table.

Fissioning nucleus	Reference	Neutron separation energy (MeV)	Photon energy range of the data in (MeV)	Number of data points
^{232}Th	36	6.43	5.85–6.35	6
^{233}U	36	5.74	5.25–5.65	5
^{234}U	37	6.84	5.15–6.34	13
^{236}U	36	6.55	5.85–6.55	8
^{238}U	36,38	6.14	5.85–6.15	4
^{237}Np	36	6.62	6.05–6.55	6
^{238}Pu	39	7.00	5.74–6.61	7
^{239}Pu	36	5.66	5.45–5.75	4
^{240}Pu	39	6.53	5.47–6.47	8
^{242}Pu	39	6.30	5.61–6.19	5
^{241}Am	36	6.66	5.85–6.65	9

lower end of the energy spectrum until a minimum in the value of χ^2 for a linear least-squares fit was obtained. The relevant details of the data used in the present analysis for various actinide nuclei along with their original references are listed in Table I.

The slopes of the near-barrier photofission cross sections obtained through the above analysis for eleven actinide nuclei are shown in Fig. 6 as a function of the neutron number. Most actinides seem to have their slopes lying between 10 and 20 mb/MeV. The slopes are seen to be somewhat lower for the actinides with smaller neutron numbers although more data are clearly needed for lighter actinides to confirm this trend conclusively. The most notable exception is that of the even-even nucleus ^{232}Th, for which even the more recent high-resolution data of Knowles *et al.*[34] also gives a slope of approximately 16–17 mb/MeV in the energy region indicated in Table I. A large value of the slope obtained for this nucleus for which a three-humped barrier has been predicted quite widely in fission literature may seem at first sight

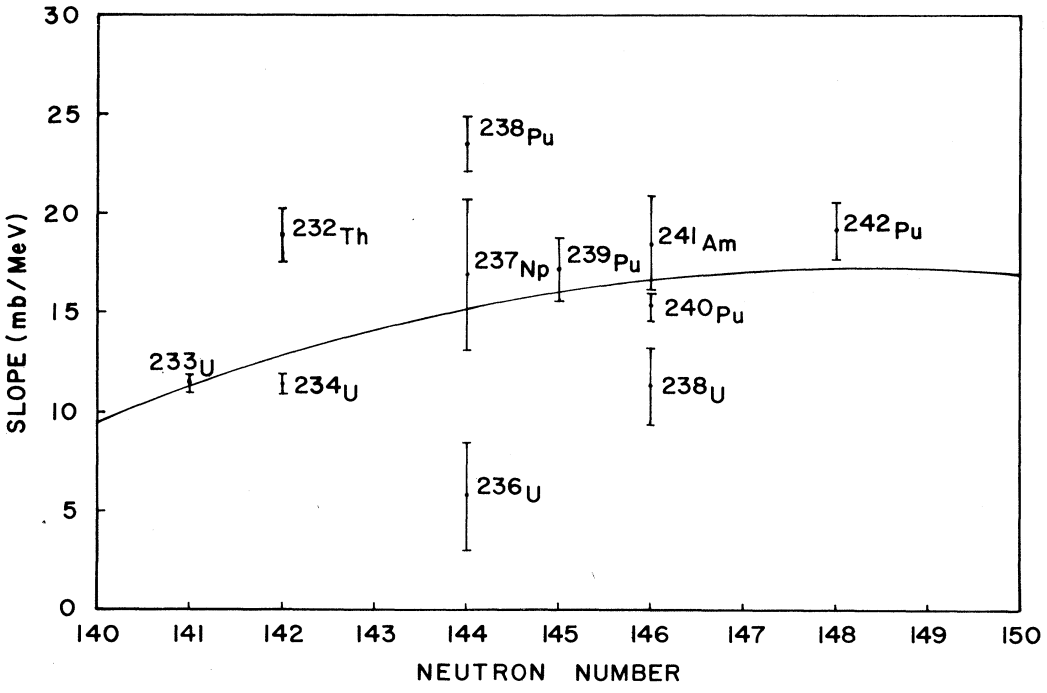

FIG. 6. Slopes of the near-barrier photofission cross sections of various actinide nuclei. The solid line represents an extrapolated least-squares fit indicating the approximate variation of the slopes with neutron numbers.

to be in contradiction with our prediction of smaller slopes for such potential shapes. However, a closer look at the predicted fission barrier shapes for the thorium nuclei reveals that as the first barrier and the second minima are too low, the effective barrier for excitations near the fission threshold is only a double-humped potential and is thus expected to yield a relatively higher value of the slope. Our analysis therefore provides further evidence in support of resolving the so-called "thorium anomaly" along the lines suggested by Möller and Nix.[4]

We also note that the slopes for the plutonium isotopes tend to be generally higher while those for the uranium isotopes are rather low as seen in detail in Fig. 7. This can be explained in terms of the predicted shapes of the double-humped barriers for these nuclei. For plutonium nuclei the outer barriers are predicted to be rather low and thus the slopes of the fission cross sections in the threshold region would be mainly determined by the single-humped inner barriers alone. However, for the uranium nuclei as both the inner and the outer barriers are predicted to be of comparable heights, the slopes would be determined by the entire double-humped barrier shapes and would thus be relatively lower. Whether the smaller slopes obtained for the uranium nuclei can be fully accounted for in terms of such broad double-humped barriers, or that three-humped barriers are warranted for their adequate explanation is not very clear, however. It is tempting nevertheless to suggest that among the actinides that we have studied in the present work, it is the uranium nuclei which may more likely exhibit well-developed three-humped fission barrier shapes in which the apparent consequences of both the second and the third minima in the potential energy surfaces may be observable. This suggestion is in agreement with the recent sketches of the fission potential barriers, for example, for ^{237}U, reported by James[28] using the turning points given by Howard and Möller.[7] More recent high-resolution experimental data[45] on (d,pf) reactions in uranium and thorium nuclei from the Saclay group also support such a conclusion. The slope for the nucleus ^{236}U, in particular, is found to be quite small. This may partly be due to a plateau-type structure in the cross-section data near 6 MeV of excitation corresponding apparently to a relatively lower fission barrier in this nucleus. The slopes of the photofission cross section data are also seen (Fig. 6) to increase linearly with the increase in nuclear charge for a given neutron number. The only exception to this systematics observed among the actinides studied in this work is ^{232}Th, and this may again be related to the special shapes of the predicted three-humped fission barriers in thorium nuclei as mentioned earlier.

IV. CONCLUSIONS

Penetrability calculations through the equivalent set(s) of the multihumped fission barriers show that the penetrability saturates to its maximum value near the top of the barriers much more slowly for a three-humped potential than that for a two-humped potential. Such a feature should lead to relatively smaller slopes for the measured fission cross sections in the threshold region for the nuclei

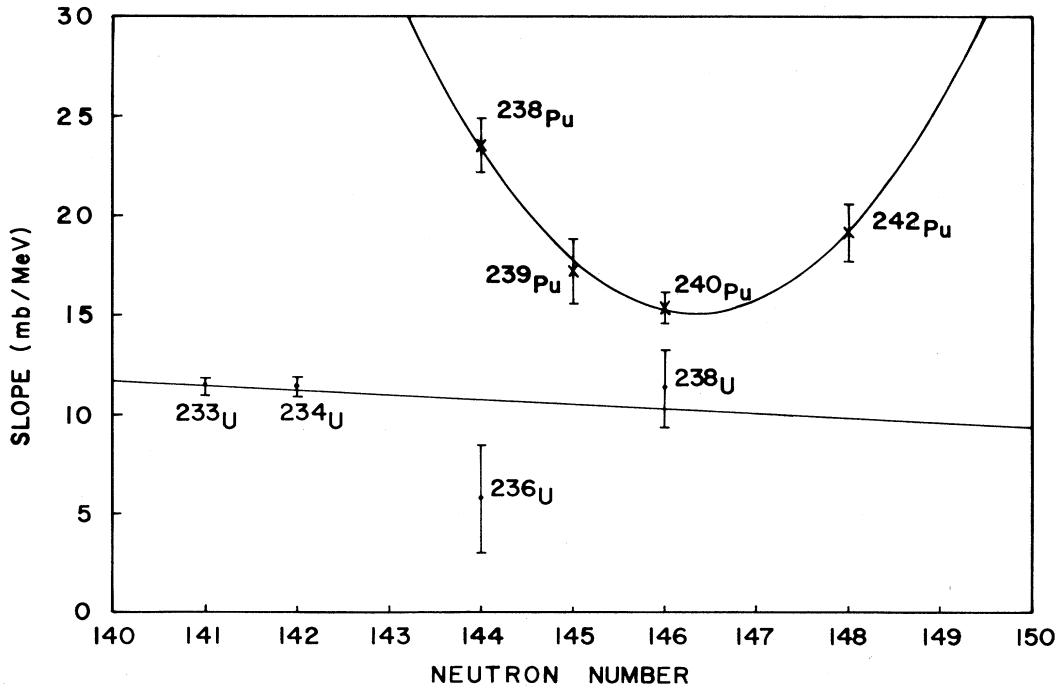

FIG. 7. Slopes of the near-barrier photofission cross sections of uranium and the plutonium isotopes. Solid lines have the same meaning as in Fig. 6.

exhibiting three-humped fission barriers. As such an expectation implies a rather strong correlation between the experimentally observed slopes of the fission probability near the top of the barrier and the nature of the fission barrier for a given nucleus, it is useful here to include a brief discussion of the assumptions as well as of the consequent limitations of our approach. In the present work we have parametrized the multihumped fission barriers by smoothly joined parabolic segments and have constructed "equivalent" three classes of barriers (one, two, and three humped) such that these all lead to approximately the same penetrability at the bottom of the potential and thus predict similar spontaneous fission halflives. This requirement of the equivalence of these three classes of barriers of approximately the same heights leads to the larger values of the curvatures near the top of the barriers for a three-humped potential than those for a comparable two-humped potential. Such differences in curvatures near the top of the barriers then lead to the different slopes in the corresponding penetrabilities.

The use of the smoothly joined parabolic segments in parametrizing the multihumped fission barriers is, of course, only an approximation. While such an approximation has worked quite well so far at least at excitations near the top of the barriers, there is no physical reason as to why the potential shapes must be exactly quadratic in the entire deformation region. Thus in reality the potential shapes could be quite different. Also the inertial parameters may vary significantly with deformation through the barrier. These factors could possibly distort the shapes of the multihumped fission barriers to such an extent that they become vastly different from smoothly joined parabolic segments. For such distorted multihumped potential shapes the correlation between the slopes of the penetrability near the top of the barrier and the nature of the fission barriers may or may not be as strong as found in our work using the parabolic potential parametrization. While it is reasonable to expect that the potential shapes in reality would be smoothly varying at least near the top of the barriers and will thus lead to results similar to those found in our present work, it is nevertheless conceivable that the real potential shapes may turn out be highly distorted or nonsmooth in certain deformation regions. With our present incomplete knowledge of the dynamics of the fission process and thus of the real shapes of the multihumped fission barriers, such a possibility cannot be completely ruled out. It is important therefore to realize that the magnitude of the slope of the fission probability near the top of the barrier alone cannot by itself determine whether the experimental barrier has two or three peaks. However, such a feature can be used as an additional information to help distinguish between such barriers in conjunction with the other expected differences such as the energies, strengths, and widths of the fission cross section resonances, and the so-called opposite parity "doublet" structures expected in a third minimum as opposed to those in the second minimum.

An analysis of the near-barrier photofission cross sections of 11 actinides studied in this work shows that the slopes tend to be generally lower for the actinides with smaller neutron numbers. A notable exception is that of ^{232}Th for which a large value obtained for the slope can be explained in terms of the predicted three-humped potential shapes with very low first barrier and the second minimum. Our analysis also shows that the uranium nuclei, in general, tend to have smaller slopes. Whether this is due to rather broad double-humped potentials with comparable heights for the two barriers predicted for such nuclei or due to the relatively well-developed three-humped fission barrier shapes is not very clear. Our results can merely be said to be consistent with the possibility of a three-peaked barrier in the uranium nuclei. As the isomeric shelf in the deep subbarrier photofission cross sections has already been well established[40–44,19] for at least two uranium isotopes (^{236}U and ^{238}U), it would be interesting to measure their photofission cross sections in the threshold region with high energy resolutions similar to that reported[34] recently for ^{232}Th. A simultaneous observation of the isomeric shelf in the deep subbarrier energy region and of the relatively undamped narrow resonances in the near-threshold fission cross sections for a given nucleus would provide compelling evidence for a three-humped fission barrier with relatively well-developed second as well as the third minima. Based on the analysis of the photofission cross sections in this work, we would like to recommend the even-even nucleus ^{236}U for such a systematic investigation.

ACKNOWLEDGMENTS

It is a pleasure to thank Dr. M. El-Fazzani and Dr. M. Khaliquzzaman for their continued interest in the work. This work is part of a research project approved and funded by the National Committee on Scientific Research, Tripoli, Libya. The financial support of the project by this agency is gratefully acknowledged. We are also grateful to the Nuclear Data Section of the International Atomic Energy Agency in Vienna for sending us a copy of the recent compilation (Ref. 35) of the measured photofission data on actinides in numerical form.

[1]V. M. Strutinsky, Nucl. Phys. **A95**, 420 (1967); **A122**, 1 (1968).
[2]J. R. Nix, Annu. Rev. Nucl. Sci. **22**, 65 (1972).
[3]H. C. Pauli and T. Ledergerber, in *Proceedings of the Third IAEA Symposium on the Physics and Chemistry of Fission, Rochester, 1973* (IAEA, Vienna, 1974), Vol. I, p. 463.
[4]P. Möller and J. R. Nix, in *Proceedings of the Third IAEA Symposium on the Physics and Chemistry of Fission, Rochester, 1973* (IAEA, Vienna, 1974), Vol. I, p. 103.
[5]M. Brack, in *Proceedings of the Fourth IAEA Symposium on the Physics and Chemistry of Fission, Julich, 1979* (IAEA, Vienna, 1980), Vol. I, p. 227.
[6]S. Bjørnholm and J. E. Lynn, Rev. Mod. Phys. **52**, 725 (1980).

[7]W. M. Howard and P. Möller, At. Data Nucl. Data Tables **25**, 219 (1980).
[8]N. Bohr and J. A. Wheeler, Phys. Rev. **56**, 426 (1939).
[9]H. C. Britt, E. Cheifetz, D. C. Hoffman, J. W. Wilhelmy, R. J. Dupzyk, and R. W. Lougheed, Phys. Rev. C **21**, 761 (1980).
[10]J. Blons, C. Mazur, D. Paya, M. Ribrag, and H. Weigmann, Phys. Rev. Lett. **41**, 1282 (1978).
[11]D. Paya, in *Proceedings of the Fourth IAEA Symposium on the Physics and Chemistry of Fission, Julich, 1979* (IAEA, Vienna, 1980), Vol. I, p. 207.
[12]J. Blons, C. Mazur, D. Paya, M. Ribrag, and H. Weigmann, Nucl. Phys. **A414**, 1 (1984).
[13]J. E. Lynn, J. Phys. G **9**, 665 (1983); Phys. Rev. C **36**, 671 (1987).
[14]A. V. Ignatyuk, N. S. Rabotnov, and G. N. Smirenkin, Phys. Lett. **29B**, 209 (1969).
[15]N. Fröman and P. O. Fröman, *JWKB Approximation* (North-Holland, Amsterdam, 1965), pp. 90–101.
[16]V. S. Masterov and A. A. Seregin, Yad. Fiz. **28**, 1195 (1978) [Sov. J. Nucl. Phys. **28**, 617 (1978)].
[17]B. S. Bhandari, Ph.D. thesis, Ohio University, 1974.
[18]B. S. Bhandari, Nucl. Phys. **A256**, 271 (1976).
[19]B. S. Bhandari, Phys. Rev. C **19**, 1820 (1979); **22**, 606 (1980).
[20]B. S. Bhandari and A. S. Al-Kharam, Research Project Report, Physics Department, University of Garyounis, Benghazi, Libya, 1986 (unpublished), and the references cited therein.
[21]T. Martinelli, E. Menapace, and A. Ventura, Lett. Nuovo Cimento **20**, 267 (1977).
[22]B. B. Back *et al.*, in *Proceedings of the Second IAEA Symposium on the Physics and Chemistry of Fission, Vienna, Austria, 1969* (IAEA, Vienna, 1969), p. 351.
[23]J. D. Cramer and J. R. Nix, Phys. Rev. C **2**, 1048 (1970).
[24]R. C. Sharma and J. N. Leboeuf, Phys. Rev. C **14**, 2340 (1976).
[25]M. Prakash and B. S. Bhandari, Phys. Rev. C **18**, 1531 (1978).
[26]L. Calabretta, A. Del Zoppo, and G. Ingrao, Nuovo Cimento A **43**, 545 (1978).
[27]D. Paya, Note Commissariat à l'Energie Atomique N-2126, 1980, p. 158.
[28]G. D. James, Comput. Phys. Commun. **40**, 375 (1986).
[29]D. L. Hill and J. A. Wheeler, Phys. Rev. **89**, 1102 (1953).
[30]H. X. Zhang, T. R. Yeh, and H. Lancman, Phys. Rev. C **34**, 1397 (1986).
[31]B. S. Bhandari and I. C. Nascimento, Nucl. Sci. Eng. **60**, 19 (1976); J. R. Huizenga, Nucl. Technol. **13**, 20 (1972).
[32]A. Bohr, in *Proceedings of the International Conference on the Peaceful Uses of Atomic Energy, Geneva, Switzerland, 1955* (United Nations, New York, 1956), Vol. 2, p. 151.
[33]R. Vandenbosch and J. R. Huizenga, *Nuclear Fission* (Academic, New York, 1973).
[34]J. W. Knowles, W. F. Mills, R. N. King, B. O. Pich, S. Yen, R. Sobie, L. Watt, T. E. Drake, L. S. Cardman, and R. L. Gulbranson, Phys. Lett. **116B**, 315 (1982).
[35]V. V. Varlamov, V. V. Surgutanov, Yu. M. Tsipenyuk, and A. P. Chernyaev, Photonuclear Data, Review: Fission of Heavy Nuclei, Centre For Photonuclear Experiments, Institute of Nuclear Physics, Moscow State University, Moscow, U.S.S.R. (1983).
[36]Yu. B. Ostapenko, G. N. Smirenkin, A. S. Soldatov, V. E. Zhuckho, and Yu. M. Tsipenyuk, Vopr. At. Nauki i Tekh. Ser.: Yadernyje Konstanty **3**, 3 (1978).
[37]L. J. Lindgren, A. S. Soldatov, and Yu. M. Tsipenyuk, Yad. Fiz. **32**, 335 (1980) [Sov. J. Nucl. Phys. **32**, 173 (1980)].
[38]V. E. Zhuchko, Yu. B. Ostapenko, G. N. Smirenkin, A. S. Soldatov, and Yu. M. Tsipenyuk, Yad. Fiz. **28**, 1185 (1978) [Sov. J. Nucl. Phys. **28**, 611 (1978)].
[39]S. P. Kapitza *et al.*, ZhETF Pis. Red. **9**, 128 (1969).
[40]C. D. Bowman, Phys. Rev. C **12**, 856 (1975); also **12**, 863 (1975).
[41]V. E. Zhuchko, A. V. Ignatyuk, Yu. B. Ostapenko, G. N. Smirenkin, A. S. Soldatov, and Yu. M. Tsipenyuk, Phys. Lett. **68B**, 323 (1977).
[42]Yu. B. Ostapenko, G. N. Smirenkin, A. S. Soldatov, and Yu. M. Tsipenyuk, Phys. Rev. C **24**, 529 (1981).
[43]Yu. B. Ostapenko, G. N. Smirenkin, A. S. Soldatov, and Yu. M. Tsipenyuk, Fiz. Elem. Chastits At. Yadra **12**, 1364 (1981) [Sov. J. Part. Nucl. **12**, 545 (1981)].
[44]Yu. M. Tsipenyuk, Yu. B. Ostapenko, G. N. Smirenkin, and A. S. Soldatov, Usp. Fiz. Nauk **144**, 3 (1984) [Sov. Phys.—Usp. **27**, 649 (1984)].
[45]J. Blons, B. Fabbro, C. Mazur, D. Paya, M. Ribrag, and Y. Patin, Nucl. Phys. **A477**, 231 (1988).